Accepted Manuscript

Effect of mechanical stimulation on the degradation of poly(lactic acid) scaffolds with different designed structures

Hengtao Shui, Quan Shi, Nicola Pugno, Qiang Chen, Zhiyong Li

PII: S1751-6161(19)30083-9

DOI: https://doi.org/10.1016/j.jmbbm.2019.04.028

Reference: JMBBM 3240

To appear in: *Journal of the Mechanical Behavior of Biomedical Materials*

Received Date: 16 January 2019

Revised Date: 12 April 2019

Accepted Date: 16 April 2019

Please cite this article as: Shui, H., Shi, Q., Pugno, N., Chen, Q., Li, Z., Effect of mechanical stimulation on the degradation of poly(lactic acid) scaffolds with different designed structures, *Journal of the Mechanical Behavior of Biomedical Materials* (2019), doi: https://doi.org/10.1016/j.jmbbm.2019.04.028.

Effect of mechanical stimulation on the degradation of poly(lactic acid) scaffolds with different designed structures

Hengtao Shui[1], Quan Shi[1], Nicola Pugno[2,3,4], Qiang Chen[1,*], Zhiyong Li[1,5*]

[1]*Biomechanics Laboratory, School of Biological Science & Medical Engineering, Southeast University, 210096, Nanjing, P.R. China*

[2]*Laboratory of Bio-Inspired & Graphene Nanomechanics, Department of Civil, Environmental and Mechanical Engineering, University of Trento, I-38123 Trento, Italy.*

[3]*School of Engineering and Materials Science, Queen Mary University of London, Mile End Road E14NS, London, UK*

[4]*Ket Lab, Edoardo Amaldi Foundation, Italian Space Agency, Via del Politecnico snc, I-11 00133 Rome*

[5]*School of Chemistry, Physics and Mechanical Engineering, Queensland University of Technology (QUT), Brisbane, QLD 4001, Australia*

***Corresponding Authors**

Associate Prof. Dr. Qiang Chen

Tel/Fax: 025-83792620

Email: chenq999@gmail.com

Prof. Dr. Zhi-Yong Li

Email: zylicam@gmail.com

Tel./Fax: +862583792620

Abstract

Biodegradability is one of the required scaffold functions for bone tissue engineering, and it is influenced by the mechanical micro-environment after scaffold implantation into body. This paper aimed to develop a mathematical model to numerically study the mechanical impact on the degradation of poly (lactic acid) (PLA) scaffolds with different designed structures. In addition, the diffused-governed autocatalysis on the scaffolds' degradation was also included, and the scaffolds' collapse time by an author-developed algorithm was determined. The results showed that an increase in mechanical stimulation led to an increase in the scaffold degradation rate. Moreover, different structures with a similar porosity shared a similar degradation tendency but had different collapse times, which is very sensitive to the diffusion coefficient of the scaffold. The present study could be helpful to understand the dynamic degradation process of PLA scaffolds, and guide the design of PLA material and scaffold structure. It may be used as a tool for the evaluation of the *in vitro* degradation performance of scaffolds.

Keywords: Scaffold degradation; Mechanical stimulation; Autocatalysis; Mathematical modeling; Finite element method.

1. Introduction

Scaffold as one of three key factors in bone tissue engineering [1] should have: (i) three-dimensional porous structure for cell growth and transport of nutrients; (ii) biocompatibility and biodegradability with a controllable degradation rate to match bone formation rate; (iii) sufficient stiffness and strength to sustain the external load during the whole bone-repair process [2-6]. Polymer is one of several biomaterials, and often employed to construct scaffolds. Thus, it has drawn much attention for biomedical applications due to its excellent processability and biodegradability [7,8].

The degradation of ester polymers is mainly caused by the hydrolysis, which is influenced by many factors, such as pH value [9], temperature, crystallinity [10], autocatalysis [11], loads [12] and loading frequency [1, 13]. The hydrolysis causes the chain scission in polymer matrix, and this embodies the decreases of the molecular weight and mechanical properties, mass loss and volumetric shrinkage of the polymer [14]. Extensive experimental studies have been conducted to explore the degradation mechanism of bulk polymer influenced by these factors. In particular, compared to the unloaded polymer samples, load was proved to accelerate the polymer degradation [12], moreover, the loading intensity and frequency influenced the bulk polymer degradation. For porous polymer scaffolds, a higher porosity induced a severer loss of mass, molecular weight and compressive modulus [15], and pore morphologies also influenced the polymer degradation [16]. In addition, the porous scaffolds are subjected to the mechanical stimulation after being implanted into human body, and according to the loading effect on the bulk polymer degradation, the mechanical

stimulation must affect the degradation of the porous polymer scaffold. Thus, both the architecture of porous scaffolds and the mechanical stimulation should be considered to design scaffolds except the well-studied chemical factors on the degradation of bulk polymers, and it is necessary to study the degradation of porous scaffolds with different architectures under mechanical stimulus.

Computational modeling and numerical simulation are useful techniques to evaluate the bulk polymer degradation. In this sense, many theoretical or numerical frameworks have been developed on the degradation [17-19]. In general, there are two main kinds of mathematical models to describe the degradation. The first is probabilistic model, which was developed on the basis of the random chain scission of polymer. The model includes Erlang probability density function [14, 20,21], Monte Carlo (MC) [22], and cellular automata (CA) methods [23]. In particular, the Erlang probability density function was popularly used to describe the bulk degradation of polymers. For example, Chen *et al.* [24] combined stochastic hydrolysis and mass transport to simulate the polymer degradation, and the model result showed a good agreement with experimental findings. The second is phenomenological model, which was based on mechanistic phenomena, such as autocatalytic reaction and crystallinity. For the autocatalysis, it is induced by the high concentration of carboxyl end groups yielded in the hydrolytic course, and the hydrolytic product cannot be timely diffused out of the polymer matrix [25]. Furthermore, as a catalyst, the acidic hydrolytic product effectively increased the local degradation rate of bulk polymers [24].

Antueunis *et al.* [26] developed a degradation model containing autocatalytic effect and predicted the average molecular weight of aliphatic polyesters during hydrolysis.

In order to address architectural effect of porous scaffolds and mechanical impact on the degradation of polymer scaffolds, this paper aims to develop a mathematical model (including the first-order Erlang stochastic hydrolysis, autocatalytic and loading effects) to explore the degradation kinetics of different scaffold architectures by employing the effective numerical method. Here, we designed three representative volumetric cells (RVCs) of three periodic scaffolds, which could be fabricated by the computer assisted design (CAD) and 3D-printing techniques [27]. By combining the developed mathematical model with the finite element method, the effect of the mechanical stimulation on the degradation of the three scaffolds was studied.

2. Degradation theory

2.1 Polymer stochastic hydrolysis

In hydrolysis, water molecules attack and break long polymer chains into water soluble products, resulting in the decrease of the molecular weight. Experiments have verified that the polymer degradation follows the pseudo-first-order kinetics [28], and a ratio $\beta(t)$ is defined to describe normalized number average molecular weight [29]:

$$\beta(t) = \frac{M_n(t)}{M_n(0)} = e^{-\lambda_0 t} \tag{1}$$

where $M_n(0)$ and $M_n(t)$ are the initial (t = 0) and instantaneous number average molecular weight, λ_0 is the degradation rate constant of polymer which is determined by polymer components. Ideally, the polymer is considered to be isotropic, and all

material points (here, a material point corresponds to a scaffold element in the following numerical models, hereafter, scaffold element is used) share an initial $M_n(0)$. However, scaffold elements have different initial porosities caused by the hydrolysis due to environment humidity, thus it is randomly assigned a value α ($0 \leq \alpha \leq 0.2$). The degradation process of the scaffold element can be considered with a delay t_{add}, which is calculated from Eq. (1) as [22]:

$$t_{add} = -\frac{\ln(1-\alpha)}{\lambda_0} \tag{2}$$

According to Gopferich *et al.* [28], the bulk degradation of polymer was a stochastic process, and each scaffold element was considered as a stochastic event. The normalized number average molecular weight described in Eq. (1) corresponds to the first-order Erlang stochastic process, and the probability density function $p(t)$ for each scaffold element is defined as:

$$p(t) = k\lambda_0 e^{-k\lambda_0 t} \tag{3}$$

with

$$k = \frac{\ln(n)}{\ln(m)}$$

where n is the number of RVC elements in the present work, and m is the referred number of the RVC elements in [22]. It is worth mentioning that k is a coefficient considering the size effect, since the number of scaffold element influences the degradation. Namely, the smaller n (*or* the larger element size), the smaller the degradation probability of a scaffold element, and this requires a longer time for a complete degradation of scaffold elements [28].

2.2 Inclusion of mechanical stimulation into the stochastic hydrolysis

Experiments revealed the effect of the mechanical stimulation on the polymer degradation [30,31]. In order to incorporate the mechanical stimulation into the degradation model, the degradation rate was re-expressed on the basis of an analysis on atomic fracture mechanism of solid polymers, and the refined the degradation rate λ_σ was proposed by Zhurkov *et al*. [32] as:

$$\lambda_\sigma = Ae^{-\frac{E_A - B\sigma}{RT}} \tag{4}$$

where A is the Arrhenius frequency factor, E_A is the activation energy breaking polymer chains, σ is the externally applied stress, B is a coefficient, R is molar gas constant and T is Kelvin temperature. Eq. (4) shows that the applied stress decreases the activation energy, and thus accelerates the polymer degradation. In particular, when σ is zero, Eq. (4) shrinks to the Arrhenius' equation, then $\lambda_\sigma = \lambda_0$. Assuming that the temperature during the hydrolysis is constant, and Eq. (4) is re-written as:

$$\lambda_\sigma = Ae^{-\frac{E_A - B\sigma}{RT}} = \lambda_0 e^{\frac{B\sigma}{RT}} \tag{5}$$

Eq. (5) indicates the relationship between the degradation of scaffold element and the mechanical stimulation. Apparently, the mechanical stimulation increases the degradation rate of polymer.

2. 3 Inclusion of autocatalysis into the stochastic hydrolysis

In vitro experiments have also demonstrated that autocatalysis plays an important role in accelerating the local hydrolysis of polymers, and thus affects the polymer degradation [33]. The mechanism of the autocatalysis is that long ester chains in polymers break into short chains with carboxyl end groups during hydrolysis, the

carboxyl end groups catalyze the hydrolysis and increase the hydrolysis rate [33]. As stated in [23], the autocatalytic effect was induced by the high concentration of carboxyl end groups, which could not be timely diffused out of the polymer matrix. Thus, in order to include the autocatalytic effect into the above stochastic hydrolysis model, the diffusion of hydrolysates was considered.

Here, the autocatalysis includes three steps, *i.e.* the release, diffusion and catalysis of hydrolysates. To describe the release-diffusion process, we employed literature-defined concentration C_{m} of hydrolysates, and the concentration of all scaffold elements is set to zero before hydrolysis (*i.e.*, $C_{\mathrm{m}}= 0$ at $t = 0$). When hydrolysis of a scaffold element starts, the hydrolysates are released. It is assumed that the polymer chain in the scaffold element is completely hydrolyzed as long as the size of the element is sufficiently small [28], and the autocatalysis has no effect on the degradation of the scaffold element when the hydrolysates were diffused out of the element. Then, the release-diffusion process of the hydrolysates in a scaffold element is modeled by Fick's second law as [34]:

$$\frac{\partial C_m}{\partial t} = \nabla(D_m \nabla C_m) + S(t) \tag{6}$$

where $S(t)$ is a term denoting the source of hydrolysates in the element, D_m is the diffusion coefficient of hydrolysates, and experimental results showed that it could be empirically determined by the degree of degradation (1-$\beta(t)$) [34], *i.e.*,

$$D_m = D_0 e^{\varphi(1-\beta(t))} \tag{7}$$

where D_0 is the initial diffusion coefficient of non-hydrolyzed polymer, φ is a material-dependent constant.

It is stated that the autocatalysis related to the concentration of hydrolysates follows an exponential relationship compared to the hydrolysis without autocatalysis. Thus, we use an exponential function to model the autocatalysis as,

$$\lambda_a = \lambda_\sigma (e^{C_m} - 1) \tag{8}$$

where λ_a is the autocatalysis-included degradation rate of a scaffold element. Finally, considering the mechanical stimulation and autocatalysis, the resulting hydrolytic rate is expressed as

$$\lambda = \lambda_\sigma + \lambda_a = \lambda_0 e^{\frac{B\sigma}{RT}} e^{C_m} \tag{9}$$

Eq. (9) becomes Eq. (5) (*or* $\lambda = \lambda_\sigma$) when the autocatalysis disappears (*i.e.*, $C_m = 0$). Correspondingly, hybrid degradation formulations for a polymer scaffold element under the mechanical stimulation and autocatalysis is expressed as:

$$\begin{cases} \beta(t) = e^{-\lambda(t+t_{add})} \\ p(t) = k\lambda e^{-k\lambda(t+t_{add})} \end{cases} \tag{10}$$

2.4 Degradation judgment of scaffold element

Based on Eq. (10), we propose two degradation conditions: (1) The normalized number average molecular weight $\beta(t)$ of each scaffold element decreases below a threshold $\beta_{threshold}$, the scaffold element is considered to be completely degraded; (2) The degradation probability $\int_t^{t+dt} p(t)dt$ is less than a randomly generated number p from 0 to 1, the scaffold element is also considered to be completely degraded [22, 29]. Under both conditions, the completely degraded element is changed into the immersing solution. Then, the criterion to judge the complete degradation of a scaffold element when either of the following conditions is satisfied,

$$\begin{cases} \beta(t) < \beta_{threshold} \\ \int_{t}^{t+\mathrm{d}t} p(t)\mathrm{d}t < p \end{cases} \tag{11}$$

The mechanical properties of polymers are related to their molecular weight [35], and they decreases exponentially during degradation process [36]. The experimental result by Tsuji [10] shows that the downtrend is similar to exponential decrease of Young's modulus. Here, the Young's modulus E_s of the scaffold element is also exponentially related to its normalized number average molecular weight ratio before its complete degradation as [29]:

$$E_s(t) = (E_s(0) - E_{solu}) \cdot \frac{e}{e-1}(1 - e^{-\beta(t)}) + E_{solu} \tag{12}$$

where $E_s(0)$ is the initial Young's modulus of the scaffold element, E_{solu} is the Young's modulus of the solution, which is a constant during degradation process. For ideal scaffold elements, their initial porosity α equals zero, we have t=0, t_{add} = 0, $\beta(0)$=1, and $E_s(t)$=$E_s(0)$. Whereas, completely degraded scaffold element has $\beta(t)$ = 0, and $E_s(t)$ = E_{solu}. Obviously, the two self-consistent conditions are satisfied. It is worth mentioning that we mainly took into account the mechanical stimulation and autocatalysis, and other factors (*e.g.* pH value, crystallinity) are ignored in the model. However, the ignored factors indeed influence the degradation of the scaffold [9, 10].

2.5 Failure of degraded scaffold under mechanical stimulation

As polymer scaffold degrades, its strength decreases. If the scaffold-solution system could not support the external applied load, the system collapses. Therefore, basing on average stresses of cross-sections of the system, we put forward a formula to calculate the average stresses to judge when the system collapses, *i.e.*,

$$\bar{\sigma}_i = \frac{\sum_{j=1}^{q_i(t)} \varepsilon_{s,crit} \times E_{s,j}(t) + \sum_{N_{layer}-q_i(t)}^{N_{layer}} \varepsilon_{solu} \times E_{solu}}{N_{layer}} \quad (13)$$

where $\bar{\sigma}_i$ is the average stress acting on the i^{th}-layered system element, $\varepsilon_{s,crit}$ is a constant critical strain of the scaffold elements, ε_{solu} is the strain of the solution element, $q_i(t)$ is a varying number of scaffold elements in the i^{th} layer, $E_{s,j}(t)$ is the Young's modulus of the j^{th} scaffold element, and N_{layer} is the element number of each layer. It is worth mentioning that $\varepsilon_{s,crit}$ is conservative, since $\varepsilon_{s,crit}$ decreases as a scaffold element degrades. Then, the calculated $\bar{\sigma}_i$ was compared with the externally applied load L_{pre}, and if any one of the layers is lower than L_{pre}, the system is considered to be collapsed, *i.e.*,

$$\bar{\sigma}_i < L_{\text{pre}} \quad (14)$$

3. Materials and Methods

3.1 Materials

PLA is biodegradable, and has been approved by Food and Drug Administration (FDA), and used in many biomedical fields [37-39]. Thus, PLA was here considered as the constituent material of porous scaffolds, and the scaffolds were immersed in solutions like body fluid, which indicated that the pores of the scaffolds were initially occupied by the solutions. PLA was treated to be isotropic and linear-elastic, and its Young's modulus and Poisson's ratio were 5 GPa [40] and 0.3 [29], respectively. The solution was also treated to be isotropic and linear-elastic but in-compressive, and its Young's modulus 10 MPa and Poisson's ratio 0.49 [29].

3.2 Scaffold structures and mesh

To investigate the effect of mechanical stimulation on the degradation processes of different scaffold structures, three periodic scaffold structures named lattice, spherical and truss were designed. The lattice and spherical structures were already presented in [41, 42]. Without loss of generality, their RVCs were treated like those in [41, 42], see upper row in Fig. 1. Geometrical sizes of the RVCs are shown in the middle row in Fig. 1. According to the geometrical parameters, their porosities were calculated as 64.8 %, 67.8 % and 64.5 %, respectively, which complied with that of trabecular bone [43]. All the RVCs were uniformly divided into 8000 (20×20×20) elements by a voxel element method, see the lower row in Fig. 1.

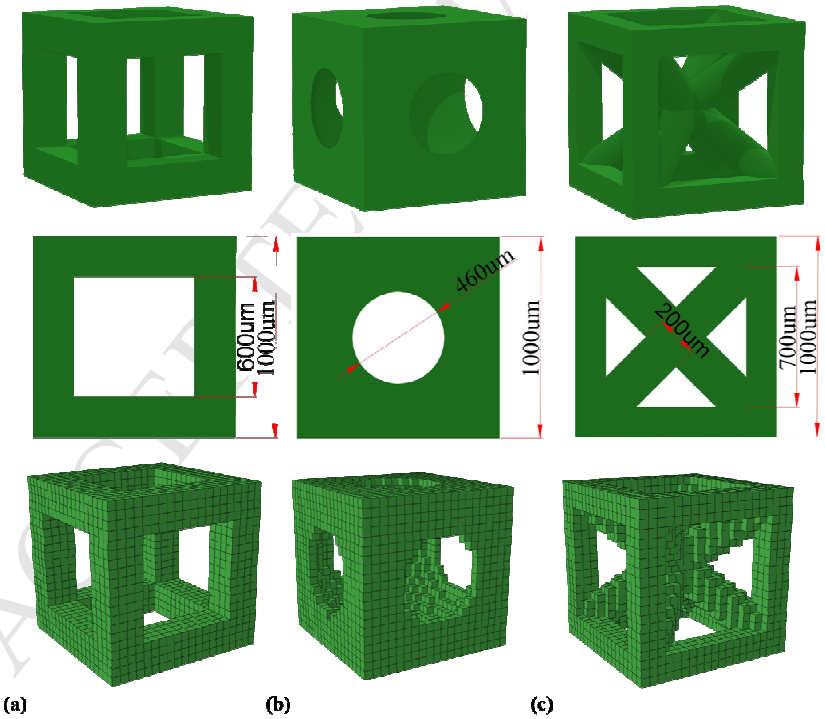

Fig. 1. Scaffold RVC structures and their geometric sizes. (a) Lattice, (b) spherical, and (c) truss RVCs

3.3 Boundary conditions

For each RVC, its bottom was fixed, and the load representing the mechanical stimulation was applied perpendicularly on its top to simulate the mechanical micro-environment in targeted sites, *e.g.* femoral shaft. To consider the influences of the surrounding RVCs and the host tissues, four lateral faces of the RVC were constrained to only allow the element nodes' to move in the loading direction. The loading history was periodic piecewise with the period 1 day, it involved an unloaded stage and a loaded stage including ascending, holding and descending sub-stages, as shown in Fig. 2. The two stages represented the exercise and the rest activities of a patient in a day, respectively. It is noted that the ascending and descending stages were set to be 0.05 day to avoid the sudden change between the unloaded and loaded stages.

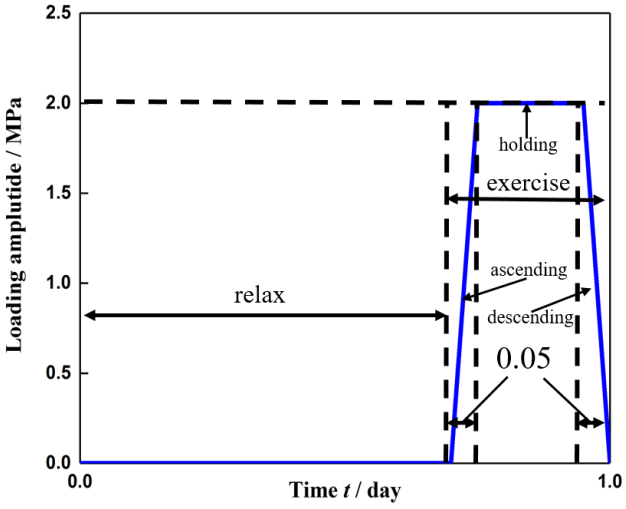

Fig. 2 Loading trapezoidal pulse in a day

3.4 Numerical implementation

The loading stress on human bones is ranging from 0.2 MPa to 4.0 MPa during normal walking [44]. Here, the loading intensities were 1.0 MPa, 1.5 MPa and 2.0 MPa, and the loading durations were 0.1, 0.2 and 0.3 day per day. Thus, nine cases

268 with the above loading intensities and durations for each RVC were treated (27
269 models for the three RVCs). The dynamic degradation process was simulated by
270 using Abaqus/Explicit (*DS SIMULIA*, USA) and coding user subroutine (VUMAT).
271 To solve the nonlinear models efficiently, Abaqus/Explicit was employed here to
272 guarantee the calculation convergence compared to Abaqus/Standard, and an
273 auto-incremental step was adopted. All the input parameters in the simulations are
274 listed in Table 1.

275 Table 1 Input parameters of simulation

Parameters		Value	Unit
Degradation rate constant	λ_0	0.0075[47]	day^{-1}
Ratio	k	0.15	-
State change threshold	$\beta_{threshold}$	0.01[29]	-
Constant	B	22[41]	J/(mol·Pa)
Gas constant	R	8.314	J/(mol·K)
Temperature	T	310	K
Initial diffusion coefficient in polymer	D_0	1.2×10^{-9}[45]	m^2/day
Material constant for diffusivity	φ	9.43[45]	-
Young's modulus of scaffold	E_s	5[40]	GPa
Young's modulus of solution	E_{solu}	0.01[29]	GPa
Poisson's ratio of scaffold	υ_s	0.3[29]	-
Poisson's ratio of solution	υ_{ECM}	0.49[29]	-
Critical strain of scaffold	$\varepsilon_{s,crit}$	5%[46]	-
Critical strain of solution	ε_{solu}	5%	-

276 **3.5 Sensitivity analysis**

277 The sensitivity analysis was also performed by varying four key parameters in
278 table 1, *i.e.*, degradation rate constant λ_0, state change threshold $\beta_{threshold}$, initial

diffusion coefficient in polymer D_0 and Young's modulus of scaffold constituent material E_s. This is because the four parameters are directly related to the degradation speed, judgment of complete degradation, autocatalysis, and selection of scaffold constituent materials. On the basis of the input values of the four parameters in Table 1, we fluctuated them by plus and minus 20%, and additional 216 models were simulated to study their sensitivity on the degradation of the scaffolds. The index S of the sensitivity was defined as,

$$S = \left| \frac{\Delta Y_i}{\Delta X_i} \right| = \left| \frac{Y_i(X_i + \alpha X_i) - Y_i(X_i - \alpha X_i)}{2\alpha X_i} \right| \quad (15)$$

where $X_i = \lambda_0, \beta_{\text{threshold}}, D_0, E_s$ are input variables, Y_i is a output variable, and α = 20% is the fluctuation of the four input variables.

4. Results and discussions

4.1 Model validation and the scaffold degradation process

To validate the proposed model, we compared the simulated average number average molecular weight $\bar{\beta}(t)$ of all residual scaffold elements in the lattice scaffold with experimental data [47, 48] in Fig. 3. Here, $\bar{\beta}(t)$ of the scaffolds was calculated through dividing the sum of $\beta(t)$ for all the residual scaffold elements by the number of the initial scaffold elements. Generally, Fig. 3 shows that the downward tendency of $\bar{\beta}(t)$ before day 30 is comparable to the literature although there exists slight deviation of experimental conditions [47, 48]. In experiment 1, PLA received no mechanical stimulation, its number average molecular weight decreases slower than others; in experiment 2, PLA received 1.0 MPa loading intensity, it is comparable to the present 1.0 MPa simulation; in experiment 3, PLA received 0.9

MPa loading intensity at 1 Hz loading frequency, despite of the lower loading intensity, the number average molecular weight decreased at a faster rate than others because of the influence of the loading frequency. Moreover, by using Eq. (1), the inversely calculated average degradation rate within the first 30 days was 2.17×10^{-2} /day, which is in the same order as the degradation rates 5.08×10^{-2} /day [49] and 4×10^{-2} /day [8], respectively. In any case, these findings demonstrate a relatively quantitative validation of the proposed model.

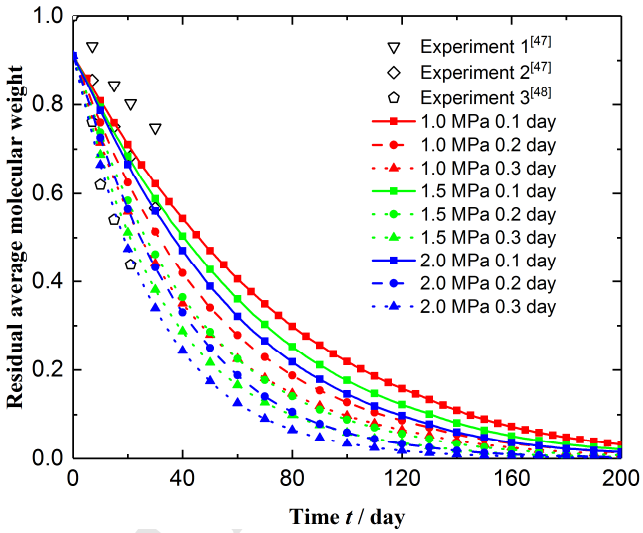

Fig. 3. Comparison of the average number average molecular weight between the simulation of the lattice scaffold and *in vitro* degradation experiments. Experiment 1: Degradation of neat-PLA immersed in Kirkland's biocorrosion media (KBM) with pH value 7.4 at 37°C under no mechanical stimulation [47]; experiment 2: Degradation of neat-PLA immersed in Kirkland's biocorrosion media (KBM) with pH value 7.4 at 37°C under loading intensity 1.0 MPa [47]; experiment 3: Degradation of neat-PLA immersed in Kirkland's biocorrosion media (KBM) with pH value 7.4 at 37°C under 0.9 MPa loading intensity at 1.0 Hz [48].

To illustrate the degradation process of the three RVCs, a specific case with the loading intensity 1.5 MPa and duration 0.2 day was presented. During their degradation processes, $\beta(t)$ at eight time points were snapshot and shown in Fig. 4. The four pillars of the three RVCs along the loading direction degraded at a faster rate than the horizontal or inclined pillars because of the higher stress. This indicates that the mechanical stimulation promotes polymer degradation. In particular, before day 50 (time point V), the vertical pillars were not completely degraded, whereas the vertical pillars were completely degraded after day 150 (time point VII).

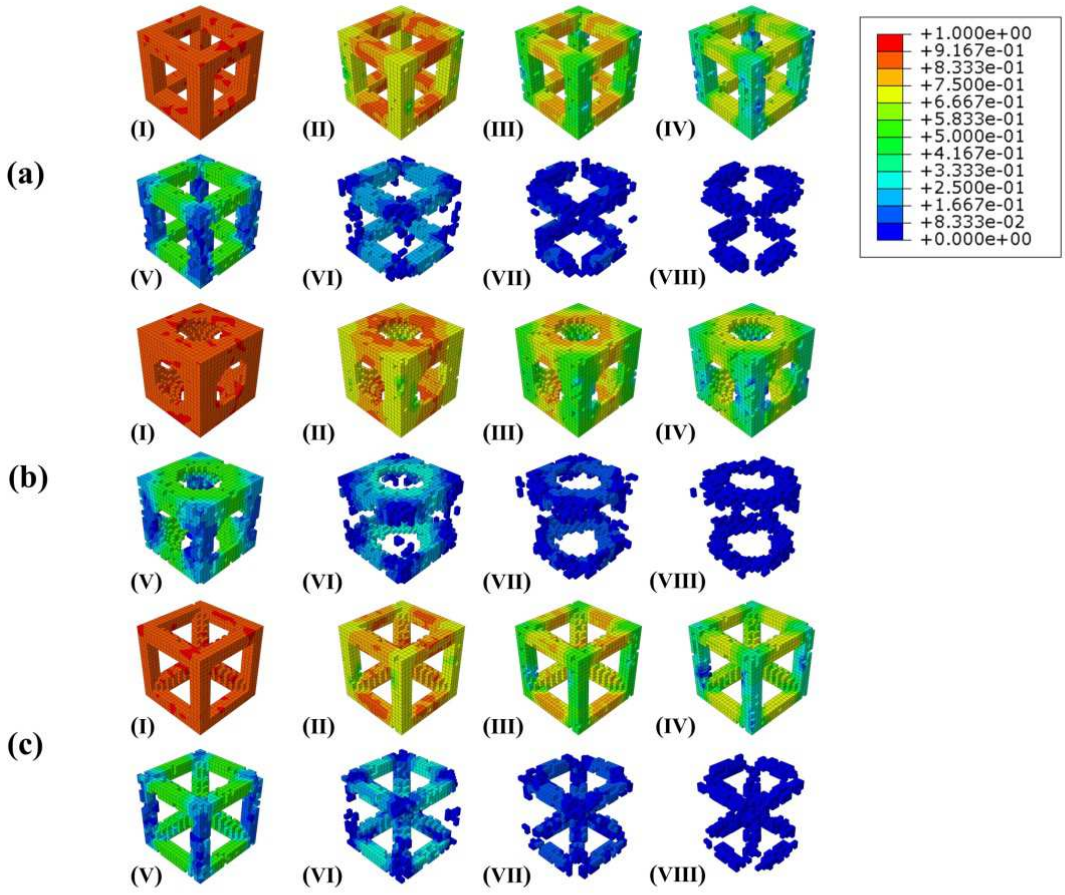

Fig. 4. The evolution of $\beta(t)$ of the three RVCs within 200 days (a) Lattice, (b) spherical, and (c) truss structures. (□. day 1, □. day 10, □. day 20, □. day 30, □. day 50, □. day 100, □. day 150, □. day 200)

4.2 Effect of mechanical stimulation on the three scaffolds

For the lattice structure, its degradation properties influenced by the mechanical stimulation are shown in Fig. 5. Generally, it shows that the nine cases with different mechanical stimulations shared a similar trend that scaffold degraded quickly during early period. For a loading duration, the higher loading intensity, the more $\bar{\beta}(t)$ decreases; while for a loading intensity, the longer loading duration, the more $\bar{\beta}(t)$ reduces, as shown in Fig. 5a. The varying volume fraction (SV/TV, SV is the volume of residual scaffold element, and TV is the sum of the volumes of scaffold and solution elements) of the residual scaffold element is shown in Fig. 5b. Different from $\bar{\beta}(t)$, SV/TV gently decreased during degradation. For example, in the case of the loading intensity 2.0 MPa at day 50, $\bar{\beta}(t)$ was about 0.40, 0.26, and 0.18 for the duration 0.1 day, 0.2 day and 0.3 day, respectively; correspondingly, SV/TV was 88.81%, 81.53% and 69.03%. This indicates that the scaffold elements were not completely degraded even though their number average molecular weight greatly decreased. Plus, increases in both loading intensity and duration greatly reduce SV/TV, *e.g.* the circled part between day 25 and day 75 for the loading intensity 2.0 MPa and duration 0.3 day in Fig. 5b. The Young's modulus of the scaffold-solution system is shown in Fig. 5c. It is worth mentioning that the Young's modulus before the system collapse was only calculated on the basis of losing supporting ability to the external load. Complying with $\bar{\beta}(t)$ and SV/TV, the Young's modulus also decreased more with a higher loading intensity or a longer loading duration, and approached to a final modulus at around 225.86 ± 20.36 MPa. Similarly, the collapse

time of the scaffold-solution system is presented in Fig. 5d, and a greater loading intensity or duration resulted in an earlier system collapse.

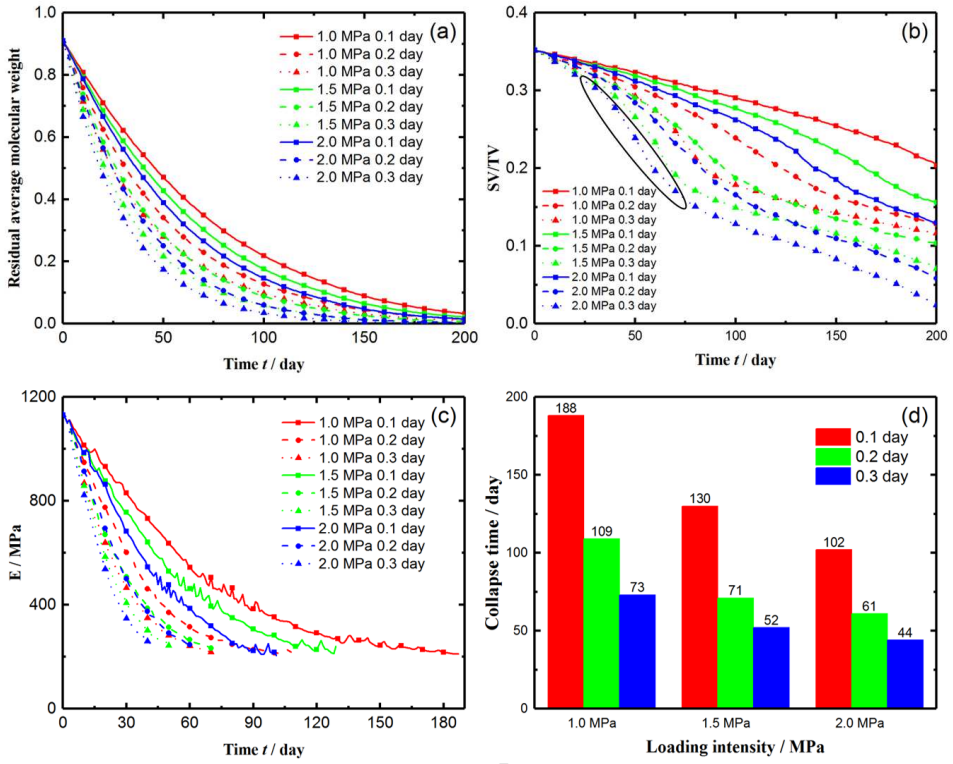

Fig. 5. Degradation of the nine cases of the lattice structure: (a) $\bar{\beta}(t)$; (b) SV/TV; (c) Young's modulus of scaffold-solution system; (d) collapsing time of the system.

For the spherical structure, its degradation properties influenced by the mechanical stimulation are shown in Fig. 6. Like the lattice structure, $\bar{\beta}(t)$, SV/TV, Young's modulus, and the collapse time were similarly influenced by the loading intensity and durations. Namely, an increase in the loading intensity and duration accelerated the spherical scaffold degradation. However, the final Young's modulus of the nine cases was 246.09 ± 28.75 MPa, which was greater than that of the lattice structure 225.86 ± 20.36 MPa. Moreover, their collapse time was 102 ± 63 day, which was smaller than those of the lattice structure (116 ± 72 day).

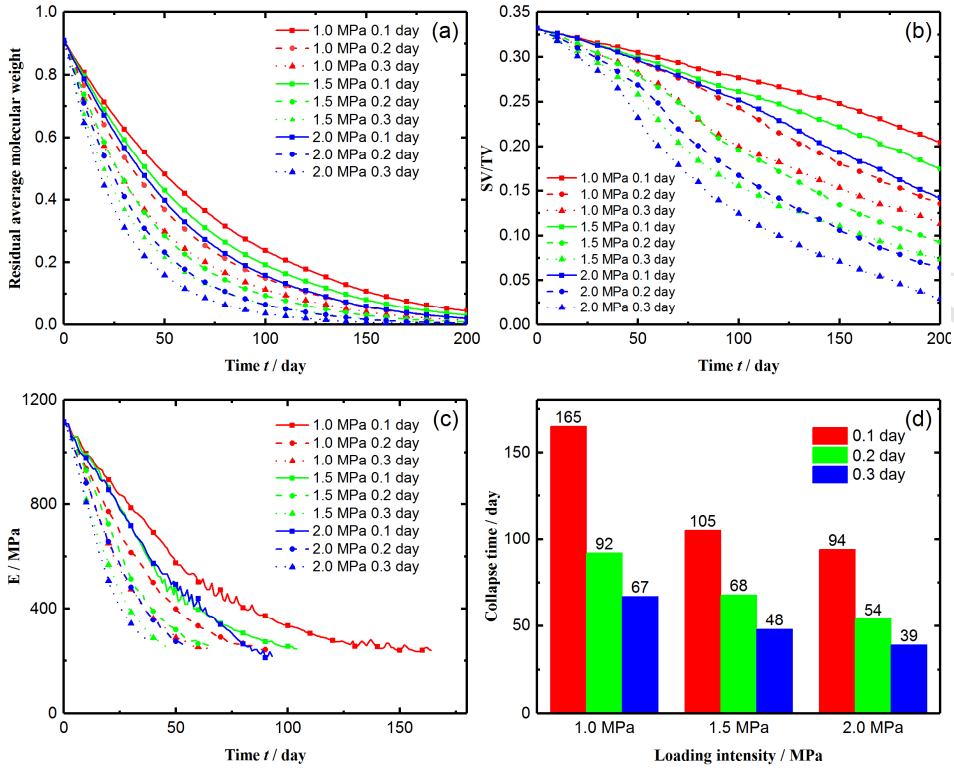

Fig. 6. Degradation of the nine cases of the spherical structure: (a) $\bar{\beta}(t)$; (b) SV/TV; (c) Young's modulus of scaffold-solution system; (d) collapsing time of the system.

For the truss structure, its degradation properties influenced by the mechanical stimulation are shown in Fig. 7. Again, like the lattice and spherical structures, $\bar{\beta}(t)$, SV/TV, Young's modulus, and the collapse time were similarly influenced by the loading intensity and durations. The increase in the loading intensity and duration speeded up the truss scaffold degradation. In particular, the final Young's modulus of the nine cases was 202.03 ± 13.67 MPa, which was smaller than that of either the lattice structure (225.86 ± 20.36 MPa) or the spherical structure (246.09 ± 28.75 MPa). However, the truss structure collapsed later than the above two structures. In particular, for the loading intensity 1.0 MPa with durations 0.1 day and 0.2 day, the structure did not collapse within the 200 days.

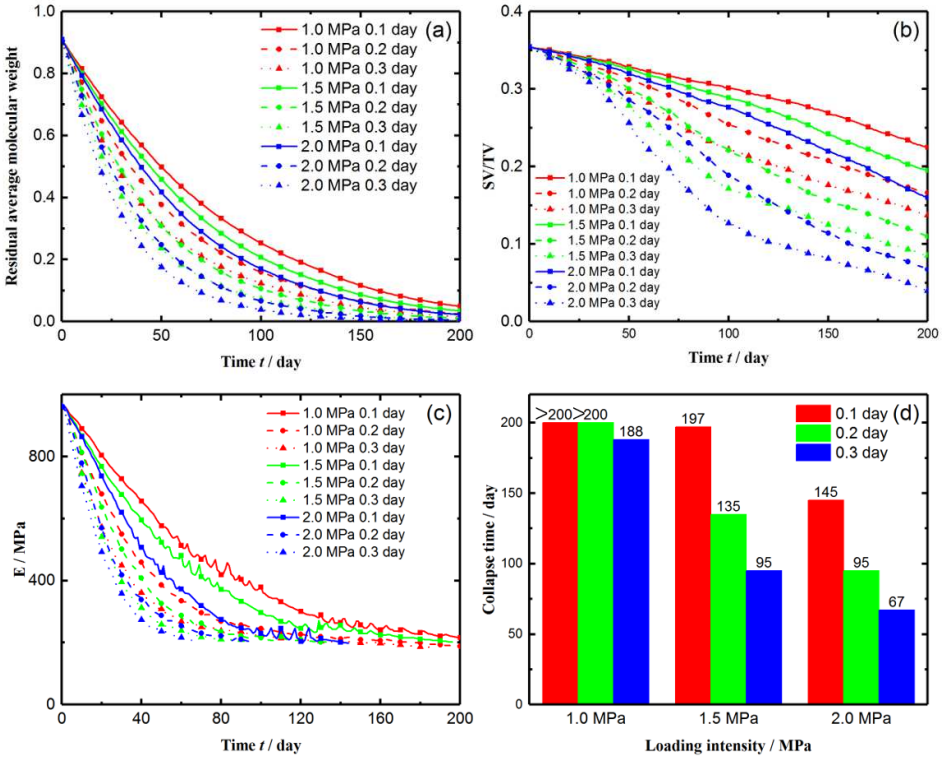

Fig. 7. Degradation of the nine cases of the truss structure: (a) $\bar{\beta}(t)$; (b) SV/TV; (c) Young's modulus of scaffold-solution system; (d) collapsing time of the system.

In all, for the three structures, these results indicate that a greater loading intensity or duration is beneficial for improving the scaffold degradation. The result is consistent with the experiments [48, 50-52]. In the sense of degradation mechanism, the mechanical stimulation decreases the activation energy of polymer hydrolysis (Eqs. (4) and (5)), which accelerates the scaffold degradation. However, Kang *et al*. [53] found that the mass loss rate of porous poly(L-lactic acid)/*β*-tricalcium phosphate composite scaffold under the static compression was slower than that of non-loading case. The inconsistence with the literature might be attributed to retarded penetration of simulated body fluid into the scaffold, which depressed the hydrolysis of the polymer component in the composite scaffold.

4.3 Comparison of the three structures

391 To illustrate different degradations of the three structures, we only compared their
392 results of the specific case with the loading intensity of 2.0 MPa and the duration of
393 0.1 day, and the comparison is shown in Fig. 8. Generally, different scaffold
394 structures weakly influence $\bar{\beta}(t)$, SV/TV, Young's modulus, but apparently
395 influence the collapse time. Particularly, $\bar{\beta}(t)$ is in the order Truss>spherical>lattice
396 (Fig. 8a). SV/TV represents the percentage of the residual scaffold elements in
397 structures. In other words, the number of the residual scaffold elements in the truss
398 structure is greater than the other two (Fig. 8b). Moreover, with the similar porosities
399 (64.8% for the lattice structure and 64.5% for the truss structure), the truss structure
400 degrades more slowly due to the shared load by oblique pillars (see Fig. 9a,c), and
401 better diffusion ability of hydrolysates, which mitigates the autocatalytic effect (see
402 Fig. 9d,f). The number of the residual scaffold element in the spherical structure is
403 smallest, and this is due to the greatest initial porosity (67.8%), but it degradation
404 mode is similar to that of the truss structure. The Young's moduli of the lattice and
405 spherical structures share a decreasing tendency, which is above that of the truss
406 structure before day 70 but below that after day 70 (Fig. 8c). This is because the truss
407 structure is more compliant due to the existence of the oblique pillars, which is mainly
408 bent instead of axial loaded under the external load. After day 70, due to its slow
409 degradation (Fig. 8a,b), the Young's modulus of the truss structure is greater than the
410 other two. As for the collapse times, they are in the order of truss>lattice>spherical
411 (Fig. 8d). The reason is that the truss structure under the external load is more stable

than the other two due to the oblique pillars (Fig. 9c), and the spherical structure has the weakest middle cross-section where the system collapses earlier (Fig. 9b).

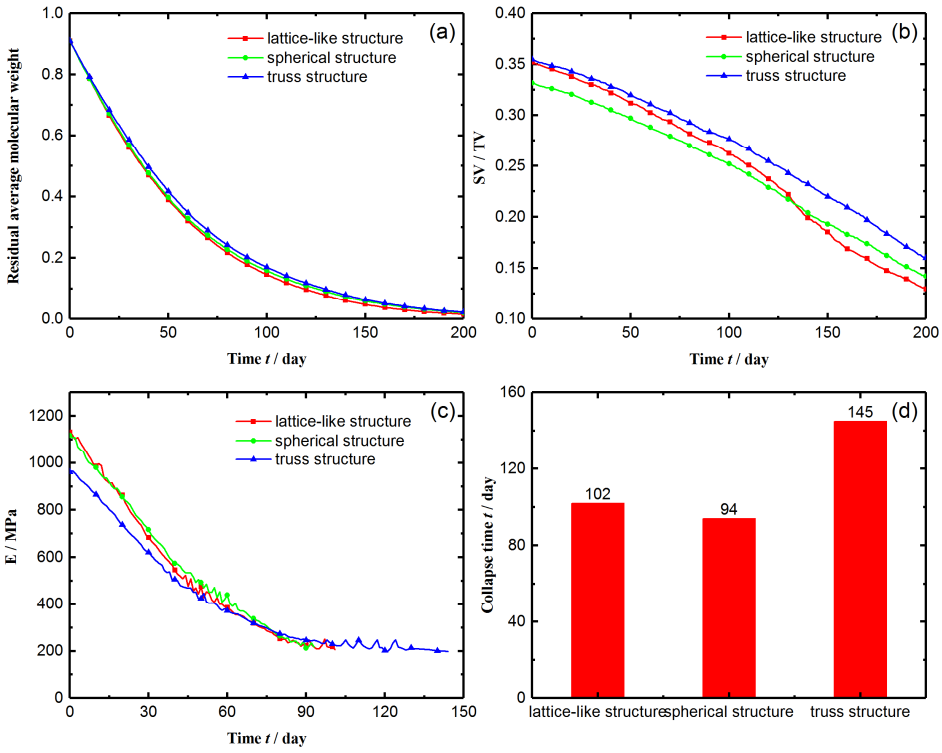

Fig. 8. Comparison of the three structures with loading intensity of 2.0 MPa and duration of 0.1 day: (a) $\bar{\beta}(t)$; (b) SV/TV; (c) Young's modulus; (d) collapsing time.

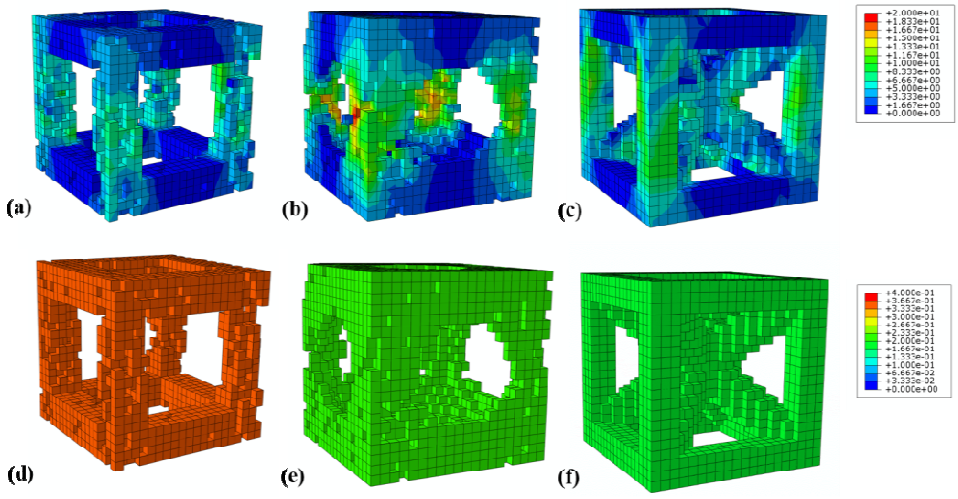

Fig. 9. Stress and C_m in the residual elements of the three structures with the loading intensity of 2.0 MPa and the duration of 0.1 day at day 50. Stresses of lattice (a), spherical (b), truss (c), and C_m of lattice (d), spherical (e), truss (f).

It is worth mentioning that the internal surface areas of the lattice, spherical, and truss structures approximately were calculated as 2.88 mm^2, 2.76 mm^2, 6.36 mm^2, respectively, thus, it seems contradictory to our intuition that the truss structure with the highest surface area should degrade faster than the other two structures. In this regard, we here considered the bulk erosion instead of surface erosion since the critical size judging bulk or surface degradations of ester polymer was greater the pillar thickness of the present structures [18], so the bulk degradation of scaffold dominated. Moreover, the mechanical stimulation and the diffusion-governed autocatalysis in the bulk degradation of all scaffold elements is the same in theory (Eq. (9)), and for the truss structure, the external load is shared by the oblique pillars and has a better diffusion ability to mitigate the autocatalytic effect. Therefore, the truss structure degrades most slowly, see Fig. 9c.

4.4 Sensitivity analysis

All the results of the additional 216 models in sensitivity analysis were reported in Supporting Materials. Due to the normalized number average molecular weight, SV/TV, and Young's modulus are varying in the degradation process. Thus we only analyzed the sensitivity by the collapse time (Y_i). Plus, in view of the huge amount of results, a specific case with the loading intensity 1.5 MPa and duration 0.2 day of the three structures were discussed. According to Eq. (15), the index S of the sensitivity are shown in Table 2. Apparently, the sensitivities of the four parameters are in the order of $D_0 > \lambda_0 > \beta_{\text{threshold}} > E_s$. This indicates that a very weak fluctuation of D_0 can result in a great variation of the collapse time.

Table 2. Index S of sensitivity of the collapse time (Y_i).

X_i	λ_0	$\beta_{threshold}$	D_0	E_s
Lattice	8.0×10^3	5.0×10^2	0.0	1.5
Spherical	9.7×10^3	0.0	4.2×10^9	2.5
Truss	1.4×10^4	4.3×10^3	4.2×10^{10}	10.5

4.5 Limitations

Indeed, there are limitations. Other factors, such as crystallization and loading frequency should be included. The crystallization [10] and loading frequency [48] influence the polymer degradation, but these issues were ignored. Second, the collapse time is calculated conservatively: on the one hand, the critical strain of scaffold element in Eq. (13) is constant. On the other hand, the solution is treated as an in-compressive solid material which retarded the collapse time. Third, the numerical result has not been fully validated through experiments which will be treated in the near future.

5. Conclusions

We developed a mathematical model to study the dynamic degradation processes of three porous scaffolds under different mechanical stimulations by including the mechanical and autocatalytic effects. The results showed that the mechanical stimulation accelerated the degradation of the PLA scaffolds. However, the degradation of the three structures with a similar porosity is weakly influenced by the mechanical stimulations except for their collapse times. Importantly, the initial diffusion coefficient is very sensitive to the collapse time induced by the scaffold

462 degradation. The present work improves our understanding of polymer degradation
463 and could be helpful for future design of suitable biodegradable scaffolds for tissue
464 engineering.

465

466 ## Acknowledgements

467 This study was supported by the Natural Science Foundation of China (NSFC)
468 (No. 31300780, 11272091, 11422222, 11772093),the Fundamental Research Funds
469 for the Central Universities (No. 2242016R30014), and partially supported by the
470 National 973 Basic Research Program of China (No. 2013CB733800) and ARC
471 (FT140101152). NMP is supported by the European Commission with the Graphene
472 Flagship Core 2 n. 785219 (WP14 “Composites”) and FET Proactive “Neurofibres” n.
473 732344 as well as by the MIUR with the “Departments of Excellence” grant L.
474 232/2016 and ARS01-01384-PROSCAN.

475

References

[1] Kang Y, Yao Y, Yin G, *et al*. A study on the in vitro degradation properties of poly (l-lactic acid)/β-tricalcuim phosphate (PLLA/β-TCP) scaffold under dynamic loading. Medical Engineering & Physics, 2009, 31(5): 589-594.

[2] Rose FRAJ, Oreffo ROC. Bone tissue engineering: hope *vs* hype. Biochemical and Biophysical Research Communications, 2002, 292(1): 1-7.

[3] Hutmacher DW. Scaffolds in tissue engineering bone and cartilage. Biomaterials, 2000, 21(24): 2529-2543.

[4] Zhang R, Ma PX. Poly (α□hydroxyl acids)/hydroxyapatite porous composites for bone-tissue engineering. I. Preparation and morphology. Journal of Biomedical Materials Research, 1999, 44(4): 446-455.

[5] Mi HY, Jing X, Turng LS. Fabrication of porous synthetic polymer scaffolds for tissue engineering. Journal of Cellular Plastics, 2015, 51(2): 165-196.

[6] Mi HY, Jing X, Yilmaz G, *et al*. In situ synthesis of polyurethane scaffolds with tunable properties by controlled crosslinking of tri-block copolymer and polycaprolactone triol for tissue regeneration. Chemical Engineering Journal, 2018, 348: 786-798.

[7] Su Y, Champagne S, Trenggono A, *et al*. Development and characterization of silver containing calcium phosphate coatings on pure iron foam intended for bone scaffold applications. Materials & Design, 2018, 148: 124-134.

[8] Helder J, Dijkstra PJ, Feijen J. In vitro degradation of glycine/DL□lactic acid copolymers. Journal of Biomedical Materials Research Part A, 1990, 24(8): 1005-1020.

[9] Zolnik BS, Burgess DJ. Effect of acidic pH on PLGA microsphere degradation and release. Journal of Controlled Release, 2007, 122(3): 338-344.

[10] Tsuji H, Mizuno A, Ikada Y. Properties and morphology of poly(L-lactide). III. Effects of initial crystallinity on long-term in vitro hydrolysis of high molecular weight poly(L-lactide) film in phosphate-buffered solution. Journal of Applied Polymer Science, 2015, 77(7): 1452-1464.

[11] Siepmann J, Elkharraz K, Siepmann F, *et al*. How autocatalysis accelerates drug release from PLGA-based microparticles: A quantitative treatment. Biomacromolecules, 2005, 6(4): 2312-2319.

[12] Fan YB, Li P, Zeng L, *et al*. Effects of mechanical load on degradation of poly(D,L-lactic acid) foam. Polymer Degradation & Stability, 2008, 93(3): 677-683.

[13] Nicodemus GD, Shiplet KA, Kaltz SR, *et al*. Dynamic compressive loading influences degradation behavior of PEG-PLA hydrogels. Biotechnology and Bioengineering, 2009, 102(3): 948-959.

[14] Göpferich A. Mechanisms of polymer degradation and erosion. Biomaterials, 1996, 17(2): 103-114.

[15] Zhang Q, Jiang Y, Zhang Y, *et al*. Effect of porosity on long-term degradation of poly (*ε*-caprolactone) scaffolds and their cellular response. Polymer Degradation and Stability, 2013, 98(1): 209-218.

[16] Wu L, Ding J. Effects of porosity and pore size on in vitro degradation of three-dimensional porous poly(D,L-lactide-*co*-glycolide) scaffolds for tissue engineering. Journal of Biomedical Materials Research Part A, 2010, 75A(4): 767-777.

519 [17] Sackett CK, Narasimhan B. Mathematical modeling of polymer erosion: Consequences for
520 drug delivery. International Journal of Pharmaceutics, 2011, 418(1): 104-114.
521 [18] Han X, Pan J. A model for simultaneous crystallisation and biodegradation of biodegradable
522 polymers. Biomaterials, 2009, 30(3): 423-430.
523 [19] Zhang T, Zhou S, Gao X, *et al.* A multi-scale method for modeling degradation of
524 bioresorbable polyesters. Acta Biomaterialia, 2017, 50: 462-475.
525 [20] von Burkersroda F, Schedl L, Göpferich A. Why degradable polymers undergo surface
526 erosion or bulk erosion. Biomaterials, 2002, 23(21): 4221-4231.
527 [21] Gopferich A, Langer R. Modeling of polymer erosion. Macromolecules, 1993, 26(16):
528 4105-4112.
529 [22] Bose SM, Git Y. Mathematical modelling and computer simulation of linear polymer
530 degradation: Simple scissions. Macromolecular Theory and Simulations, 2004, 13(5):
531 453-473.
532 [23] Arifin DY, Lee LY, Wang CH. Mathematical modeling and simulation of drug release from
533 microspheres: Implications to drug delivery systems. Advanced Drug Delivery Reviews,
534 2006, 58(12-13): 1274-1325.
535 [24] Chen Y, Zhou S, Li Q. Mathematical modeling of degradation for bulk-erosive polymers:
536 applications in tissue engineering scaffolds and drug delivery systems. Acta Biomaterialia,
537 2011, 7(3): 1140-1149.
538 [25] Siparsky GL, Voorhees KJ, Miao F. Hydrolysis of polylactic acid (PLA) and
539 polycaprolactone (PCL) in aqueous acetonitrile solutions: autocatalysis. Journal of
540 Environmental Polymer Degradation, 1998, 6(1): 31-41.

[26] Antheunis H, van der Meer JC, de Geus M, *et al*. Autocatalytic equation describing the change in molecular weight during hydrolytic degradation of aliphatic polyesters. Biomacromolecules, 2010, 11(4): 1118-1124.

[27] Gómez S, Vlad MD, López J, *et al*. Design and properties of 3D scaffolds for bone tissue engineering. Acta Biomaterialia, 2016, 42: 341-350.

[28] Göpferich A. Polymer bulk erosion. Macromolecules, 1997, 30(9): 2598-2604.

[29] Shi Q, Chen Q, Pugno N, *et al*. Effect of rehabilitation exercise durations on the dynamic bone repair process by coupling polymer scaffold degradation and bone formation. Biomechanics and Modeling in Mechanobiology, 2018, 17(3): 763-775.

[30] Thompson DE, Agrawal CM, Athanasiou K. The effects of dynamic compressive loading on biodegradable implants of 50–50% polylactic acid–polyglycolic acid. Tissue Engineering, 1996, 2(1): 61-74.

[31] Li Y, Chu Z, Li X, *et al*. The effect of mechanical loads on the degradation of aliphatic biodegradable polyesters. Regenerative Biomaterials, 2017, 4(3): 179-190.

[32] Zhurkov SN, Korsukov VE. Atomic mechanism of fracture of solid polymers. Journal of Polymer Science: Polymer Physics Edition, 1974, 12(2): 385-398.

[33] Lam CXF, Savalani MM, Teoh SH, *et al*. Dynamics of in vitro polymer degradation of polycaprolactone-based scaffolds: accelerated versus simulated physiological conditions. Biomedical Materials, 2008, 3(3): 034108.

[34] Thombre AG, Himmelstein KJ. A simultaneous transport-reaction model for controlled drug delivery from catalyzed bioerodible polymer matrices. AIChE Journal, 1985, 31(5): 759-766.

562 [35] Nunes RW, Martin JR, Johnson JF. Influence of molecular weight and molecular weight
563 distribution on mechanical properties of polymers. Polymer Engineering & Science, 1982,
564 22(4): 205-228.
565 [36] Blaker JJ, Nazhat SN, Maquet V, *et al*. Long-term in vitro degradation of PDLLA/Bioglass®
566 bone scaffolds in acellular simulated body fluid. Acta Biomaterialia, 2011, 7(2): 829-840.
567 [37] Tyler B, Gullotti D, Mangraviti A, *et al*. Polylactic acid (PLA) controlled delivery carriers for
568 biomedical applications. Advanced Drug Delivery Reviews, 2016, 107: 163-175.
569 [38] Mi HY, Salick MR, Jing X, *et al*. Characterization of thermoplastic polyurethane/polylactic
570 acid (TPU/PLA) tissue engineering scaffolds fabricated by microcellular injection molding.
571 Materials Science and Engineering: C, 2013, 33(8): 4767-4776.
572 [39] Mi HY, Jing X, Napiwocki BN, *et al*. Biocompatible, degradable thermoplastic polyurethane
573 based on polycaprolactone-block-polytetrahydrofuran-block-polycaprolactone copolymers
574 for soft tissue engineering. Journal of Materials Chemistry B, 2017, 5(22): 4137-4151.
575 [40] Middleton JC, Tipton AJ. Synthetic biodegradable polymers as orthopedic devices.
576 Biomaterials, 2000, 21(23): 2335-2346.
577 [41] Adachi T, Osako Y, Tanaka M, *et al*. Framework for optimal design of porous scaffold
578 microstructure by computational simulation of bone regeneration. Biomaterials, 2006,
579 27(21): 3964-3972.
580 [42] Sanz-Herrera JA, García-Aznar JM, Doblaré M. On scaffold designing for bone regeneration:
581 a computational multiscale approach. Acta Biomaterialia, 2009, 5(1): 219-229.
582 [43] Ding M, Hvid I. Quantification of age-related changes in the structure model type and
583 trabecular thickness of human tibial cancellous bone. Bone, 2000, 26(3): 291-295.

584 [44] Urban JPG. The chondrocyte: a cell under pressure. Rheumatology, 1994, 33(10): 901-908.

585 [45] Gleadall A, Pan J, Kruft MA, *et al.* Degradation mechanisms of bioresorbable polyesters.
586 Part 1. Effects of random scission, end scission and autocatalysis. Acta Biomaterialia, 2014,
587 10(5): 2223-2232.

588 [46] Nishida M, Yamaguchi M, Todo M, *et al*. Evaluation of dynamic compressive properties of
589 PLA polymer blends using split Hopkinson pressure bar. International Conference on the
590 Mechanical and Physical Behaviour of Materials Under Dynamic Loading, 2009, 1: 909-915.

591 [47] Li X, Chu C, Wei Y, *et al*. In vitro degradation kinetics of pure PLA and Mg/PLA composite:
592 Effects of immersion temperature and compression stress. Acta Biomaterialia, 2017, 48:
593 468-478.

594 [48] Li X, Qi C, Han L, *et al.* Influence of dynamic compressive loading on the in vitro
595 degradation behavior of pure PLA and Mg/PLA composite. Acta Biomaterialia, 2017, 64:
596 269-278.

597 [49] Tsuji H, Eto T, Sakamoto Y. Synthesis and hydrolytic degradation of substituted poly
598 (DL-Lactic Acid)s. Materials, 2011, 4(8): 1384-1398.

599 [50] Yang Y, Zhao Y, Tang G, *et al*. In vitro degradation of porous poly (l-lactide-co-glycolide) /
600 β-tricalcium phosphate (PLGA/β-TCP) scaffolds under dynamic and static conditions.
601 Polymer Degradation and Stability, 2008, 93(10): 1838-1845.

602 [51] Smutz WP, Daniels AU, Andriano KP, *et al.* Mechanical test methodology for environmental
603 exposure testing of biodegradable polymers. Journal of Applied Biomaterials, 1991, 2(1):
604 13-22.

[52] Tong L, White JR. Photo-oxidation of thermoplastics in bending and in uniaxial compression. Polymer Degradation and Stability, 1996, 53(3): 381-396.

[53] Kang YQ, Yin GF, Luo L, *et al.* Effects of mechanical stress on the in vitro degradation of porous composite scaffold for bone tissue engineering. Key Engineering Materials, 2007, 342: 273-276.